Fragment-Based Discovery of a Dual pan-RET/VEGFR2 Kinase Inhibitor Optimized for Single-Agent Polypharmacology**

Brendan Frett, Francesca Carlomagno, Maria Luisa Moccia, Annalisa Brescia, Giorgia Federico, Valentina De Falco, Brittany Admire, Zhongzhu Chen, Wenqing Qi, Massimo Santoro, and Hong-yu Li**

Abstract: Oncogenic conversion of the RET (rearranged during transfection) tyrosine kinase is associated with several cancers. A fragment-based chemical screen led to the identification of a novel RET inhibitor, Pz-1. Modeling and kinetic analysis identified Pz-1 as a type II tyrosine kinase inhibitor that is able to bind the "DFG-out" conformation of the kinase. Importantly, from a single-agent polypharmacology standpoint, Pz-1 was shown to be active on VEGFR2, which can block the blood supply required for RET-stimulated growth. In cell-based assays, 1.0 nM of Pz-1 strongly inhibited phosphorylation of all tested RET oncoproteins. At 1.0 mg kg^{-1} day^{-1} per os, Pz-1 abrogated the formation of tumors induced by RET-mutant fibroblasts and blocked the phosphorylation of both RET and VEGFR2 in tumor tissue. Pz-1 featured no detectable toxicity at concentrations of up to 100.0 mg kg^{-1}, which indicates a large therapeutic window. This study validates the effectiveness and usefulness of a medicinal chemistry/polypharmacology approach to obtain an inhibitor capable of targeting multiple oncogenic pathways.

Targeted treatments are aimed at providing cancer patients with agents, such as tyrosine kinase inhibitors (TKIs), that are designed to target tumor cells or the tumor microenvironment. Unfortunately, drug resistance to TKIs invariably develops owing to the inability to sustainably knock out tumor-survival pathways or to maintain activity on the target as additional mutations form.[1–3] Resistance can be reduced by identifying, through medicinal chemistry/polypharmacology[4] (MCP), personalized TKIs with optimized inhibitory profiles for critical disease-promoting kinases, including crucial mutant targets. A single agent with an appropriate inhibitory profile can possess the benefits of combination therapy and effectively target tumor growth while preventing resistance formation.[5] Herein, we have applied MCP using a novel fragment-based approach to identify a pan-RET/VEGFR2 dual inhibitor (RET = rearranged during transfection, VEGFR2 = vascular endothelial growth factor receptor 2). The inhibitor is capable of effectively treating both the parenchyma (RET) and stroma (VEGFR2) of RET-driven tumors, while maintaining activity on all tested RET oncogene mutants.

RET is a transmembrane tyrosine kinase (TK) receptor that has emerged as a molecular target for the treatment of several cancer types, primarily medullary thyroid carcinoma (MTC).[6–8] In a tumor environment, VEGFR2-mediated angiogenesis provides oxygen and the nutrients necessary for RET oncogenic signaling. Vandetanib (Caprelsa) and cabozantinib (Cometriq) were originally discovered as inhibitors of different tyrosine kinases, including VEGFR2, and have been approved to treat MTC because of their capability to prolong progression-free survival compared to placebo treatments.[9, 10] Both agents possess activity on wild-type and oncogenic RET mutants, but not on RET gatekeeper (V804) mutants. Therefore, our goal was to implement the concept of single-agent polypharmacology (SAP) to design a RET/VEGFR2 dual inhibitor that is selective and equipotent on both kinases, including clinically relevant mutants, to provide a new targeted agent for RET-driven cancers.

[*] B. Frett,[+] Z. Chen, H.-y. Li
    Medicinal Chemistry Division, Pharmacology and Toxicology
    College of Pharmacy, The University of Arizona
    1703 E. Mabel, Tucson, AZ 85721 (USA)
    E-mail: hongyuli@pharmacy.arizona.edu

    F. Carlomagno,[+] M. L. Moccia, A. Brescia, G. Federico, V. De Falco,
    M. Santoro
    Dipartimento di Medicina Molecolare e Biotecnologie Mediche
    Università di Napoli "Federico II"/Istituto di Endocrinologia ed
    Oncologia Sperimentale del CNR
    80131 Naples (Italy)
    E-mail: masantor@unina.it

    B. Admire
    Pharmaceutical Sciences, College of Pharmacy
    The University of Arizona
    1703 E. Mabel, Tucson, AZ 85721 (USA)

    W. Qi
    The University of Tennessee, Health Science Center
    Memphis, TN 38163 (USA)

    B. Frett,[+] H.-y. Li
    Synactix Pharmaceuticals, Inc.
    6510 N. Camino Arturo, Tucson, AZ 85718 (USA)
    E-mail: contact@synactixpharma.com

    Z. Chen
    Chongqing University of Arts and Sciences
    Chongqing, 402160 (China)

  [+] These authors contributed equally to this work.

Compound design was largely guided by computational modeling and the use of a modified fragment-based approach. For the modeling studies, the RET tyrosine kinase domain that had previously been crystallized in complex with small type I inhibitors, which bind to the "DFG-in" (native active fold) conformation of the kinase, was used.[11] To search for more selective RET TKIs, a "DFG-out" (inactive fold) homology model capable of interacting with type II inhibitors was generated by utilizing an available RET sequence (PDB: 2IVU) and a VEGFR2 DFG-out template (PDB: 2OH4; see the Supporting Information, Figure S1). The model displayed the appropriate shift in the DFG loop, which opened the allosteric pocket and was used for molecular docking and structure–activity relationship (SAR) studies.

Kinase fragment libraries are traditionally composed of small hinge binders that consist of one or two fused aryl and/or heteroaryl ring systems with hydrogen-bond donors or acceptors. Such fragments are highly polar and can aggregate at the millimolar concentrations that are often necessary to achieve activity in a biochemical fragment screen. As a result, achieving a good noise-to-signal ratio is a major challenge with this method. A kinase-directed fragment (KDF) library was designed to enhance the sensitivity and more effectively interrogate binding functionalities at a kinase hinge (Figure 1).[12] This KDF library contained a diverse set of

Table 1: Compound activities on RET, VEGFR2, and RET^V804M.

Compound	RET	VEGFR2	RET^V804M
1	(28 ± 3) %,[b] (63 ± 5) %[c]	(59 ± 3) %[c]	–
1a	(18.2 ± 0.81) μM[a]	(89 ± 4) %[c]	–
2	(2.1 ± 0.24) μM[a]	(93 ± 2) %[c]	–
3	0.006 μM[d]	0.018 μM[d]	0.006 μM[d]
3b	(0.047 ± 0.007) μM[a]	(97 ± 2) %[c]	–
Pz-1 (**4**)	< 0.001 μM[a]	< 0.001 μM[a]	< 0.001 μM[a]

[a] IC$_{50}$ values were determined using a microfluidic separation based assay. The data represent means from at least three independent experiments. [ATP] = 190 μM. [b] Residual activity at 100.0 μM determined in triplicate. [ATP] = 190 μM. [c] Residual activity at 20.0 μM determined in triplicate. [ATP] = 190 μM. [d] K_d values were determined using an active-site-directed competition binding assay that was outsourced to KINOMEScan.
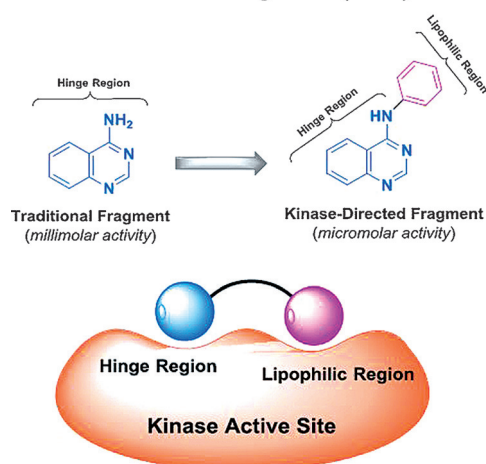

Kinase-Directed Fragment (KDF) Library

Figure 1. Concept for increasing the potency and mitigating the aggregation liability in a novel kinase fragment library by using kinase-directed fragments (KDFs). KDFs are composed of a hinge region tethered to a lipophilic region for increased potency.

heterocyclic hinge-region binders along with moieties that can engage lipophilic pockets or the ribose sugar pocket. Accordingly, KDFs have larger molecular weights and are generally more active than the fragments contained in traditional libraries, permitting screening in the micromolar range. From such a library, a benzimidazole analogue was identified as a promising starting platform for a RET TKI (compound **1**; Figure 2A, Table 1). Compound **1** effectively inhibited RET at both 100.0 and 20.0 μM (Table 1). Molecular modeling of

compound **1** in the RET kinase showed that heterocyclic substitution at the bromine would be tolerated (compound **1a**; Figure 2A,D). This region is solvent-exposed and occupied by the adenine ring system when ATP is bound. Compound **1a** displayed improved RET potency with an IC$_{50}$ value of 18.2 ± 0.81 μM (Table 1). Further modeling showed that the DFG pocket of the RET kinase could be accessed with the addition of a bridge connected to an allosteric group such as a *meta*-trifluoromethylphenyl moiety (compound **2**; Figure 2A,C); compound **2** indeed showed improved potency against the RET kinase with an IC$_{50}$ value of 2.1 ± 0.24 μM (Table 1). The combination of SAR information from compounds **1**, **1a**, and **2** resulted in compound **3** with RET, VEGFR2, and RET^V804M K_d values of 0.006, 0.018, and 0.006 μM, respectively (Table 1). Compound **3** was further optimized on RET and VEGFR2 at both the allosteric region and the 5-position of the benzimidazole, which led to compound **4** (Pz-1; Figure 2A,E, see also Figure S2). Specifically, a pyrazole at the solvent region and an isoxazole in the allosteric pocket were highly favored for strong RET inhibition. Pz-1 was found to be active on RET, RET mutants, and VEGFR2 with similar IC$_{50}$ values (all < 1.0 nM, Table 1). The equal potency was later confirmed in cell-based assays. Pz-1 is expected to simultaneously block VEGFR2-mediated nutrient accumulation and RET/RET-mutant cell proliferation.

Molecular modeling demonstrated that Pz-1 could bind RET and VEGFR2 with different binding geometries because of free rotation of the methylene linker that bridges the hinge region to the allosteric pocket (Figure S3). In complex with RET, the linker amide is in the "up" position, whereas with VEGFR2, the linker amide is in the "down" position. The free rotation in Pz-1 presumably helps the inhibitor to achieve similar potencies on RET, RET mutants, and VEGFR2. Accordingly, Pz-1 exhibited IC$_{50}$ values of < 1.0 nM for both wild-type RET and VEGFR2 kinases (Table 1). Computational modeling of Pz-1 within the RET kinase showed that binding occurred > 3.5 Å away from the gatekeeper residue (V804; Figure 2E). As a result of the large binding distance from the gatekeeper region, Pz-1 exhibited a strong affinity for the gatekeeper mutant RET^V804M (Table 1). RET^V804M is
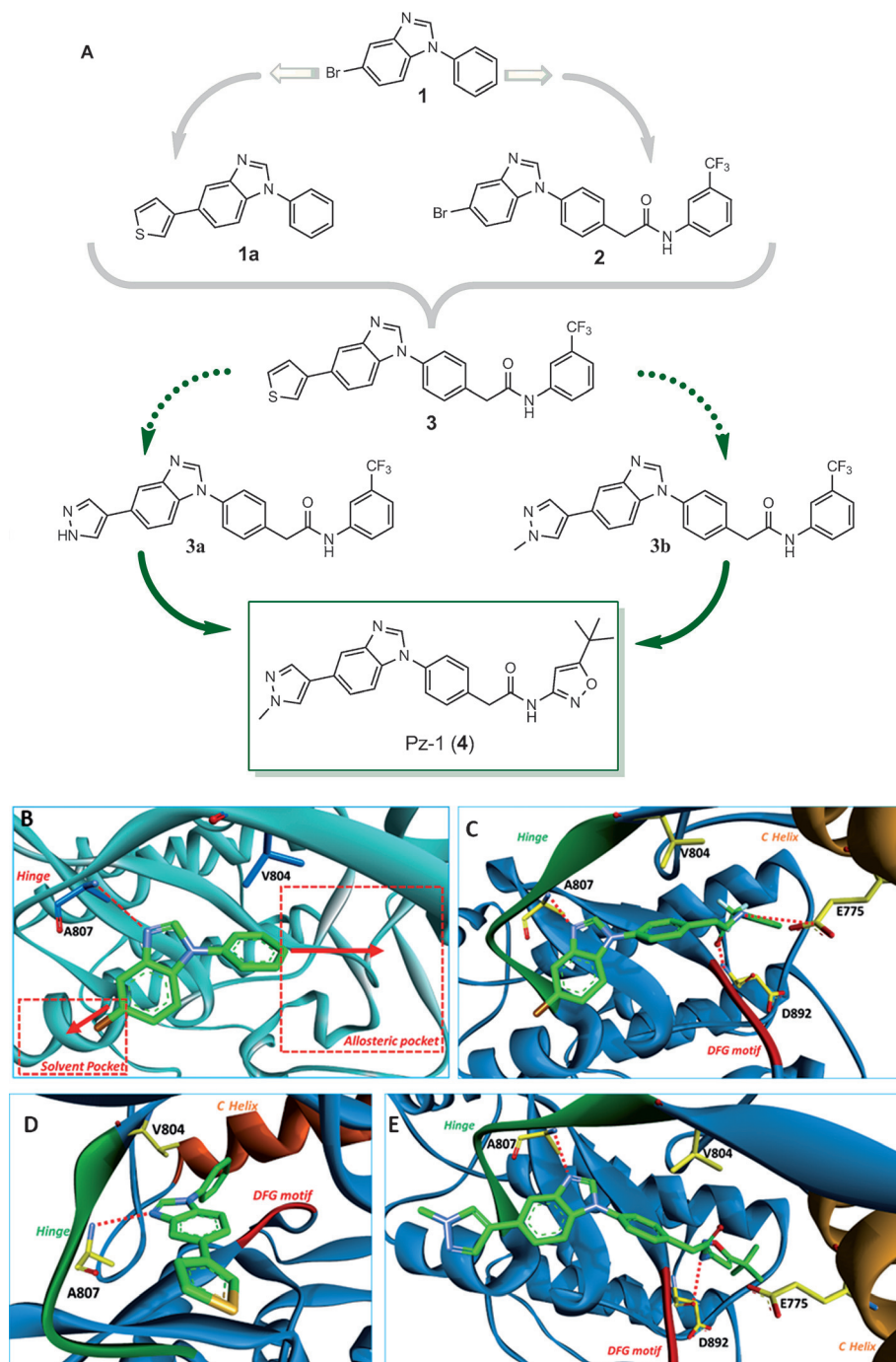
Figure 2. Design and molecular modeling of Pz-1 (compound **4**). A) Progression from KDF **1** to clinical candidate Pz-1 (**4**). From compound **1**, the solvent region as well as the allosteric pocket were optimized to furnish compounds **1a** and **2**, respectively. Compounds **1a** and **2** were combined to generate lead candidate **3**. Further medicinal-chemistry efforts generated the optimized RET/VEGFR2 dual inhibitor Pz-1 (**4**). B) Computational modeling of compound **1** in the RET DFG-in crystal structure (PDB: 2IVU). The modeling identified two possible points for optimization: 1) the solvent pocket and 2) the allosteric pocket. C) Computational modeling of compound **2** in the RET DFG-out homology model. Compound **2** is predicted to bind to A807 of the hinge and form two hydrogen bonds on the RET bridge. One hydrogen bond is predicted to form with D892 of the DFG motif and the other one with E775 of the C helix at the back of the allosteric pocket. The interactions with an aspartic acid of the DFG motif and a glutamic acid residue of the C helix are similar to the interactions of imatinib with c-ABL (PDB: 3K5V). D) Computational modeling of compound **1a** in the RET DFG-in crystal structure (PDB: 2IVU). Substitution at the solvent pocket is predicted to be tolerated. E) Computational modeling of Pz-1 (**4**) in the RET DFG-out homology model. Pz-1 is predicted to make a contact with D892 at the DFG loop but not with E775 of the C helix. The binding geometry of Pz-1 places the compound far away from the gatekeeper region avoiding a steric clash with bulky residues at position 804.

refractory to both vandetanib and cabozantinib,[13] suggesting that Pz-1 has a novel RET binding mode. Vandetanib is located approximately 2.8 Å away from the gatekeeper residue (V804), almost 1.0 Å closer than Pz-1; the vandetanib affinity for RET^{V804M} and RET^{V804L} is likely abrogated because of steric hindrance with the larger mutant residues at the gatekeeper region.

To identify the type of inhibition exhibited, the ATP K_m value for RET was determined and found to be 12.00 ± 0.26 μM (Figure S4). As the utilized RET kinase assay is not suitable for precisely determining the activity of highly potent inhibitors such as Pz-1 ($IC_{50} < 1.0$ nM), compound **3b** was selected for inhibition studies because its activity was within the limits of assay reliability. The IC_{50} value of **3b** was determined at ATP concentrations of 6.2, 12.5, 50.0, and 100.0 μM. Although there was a slight increase in IC_{50} values with an increase in ATP concentration, compound **3b** remained a strong inhibitor at highly saturating ATP concentrations (Table 2, see also Figure S5). This finding suggests that the benzimidazole scaffold of Pz-1 is somewhat competitive with ATP for binding as inhibition was relieved but not completely abrogated.

In cell-based assays, consistent with the biochemical SAR studies, Pz-1 displayed a higher RET inhibitory activity towards oncogenic RET^{C634R} than its predecessor compounds (**1**, **2**, and **3**; Figure 3 A). Pz-1 was also highly effective against other common oncogenic RET point mutants, including RET^{M918T}, the most common mutant associated with the inherited multiple endocrine neoplasia type 2B (MEN2B) syndrome and sporadic MTC, as well as RET^{V804M} and RET^{V804L} mutants (Figure 3 B). Moreover, Pz-1 was also confirmed to be equally potent on VEGFR2, inhibiting VEGFA-induced VEGFR2 phosphorylation at a 1.0 nM dose in transfected HEK293 cells and, at the endogenous level, in HUVEC cells (Figure 3 C, see also Figure S6).

Table 2: Inhibition values of compound **3b**.[a]

ATP [μM]	6.2	12.5	50.0	100.0
IC$_{50}$ [nM]	20.6 ± 4.3	27.4 ± 1.1	33.7 ± 3.18	46.5 ± 6.9

[a] IC$_{50}$ values were determined using a microfluidic separation based assay. The data represent means from at least three independent experiments.
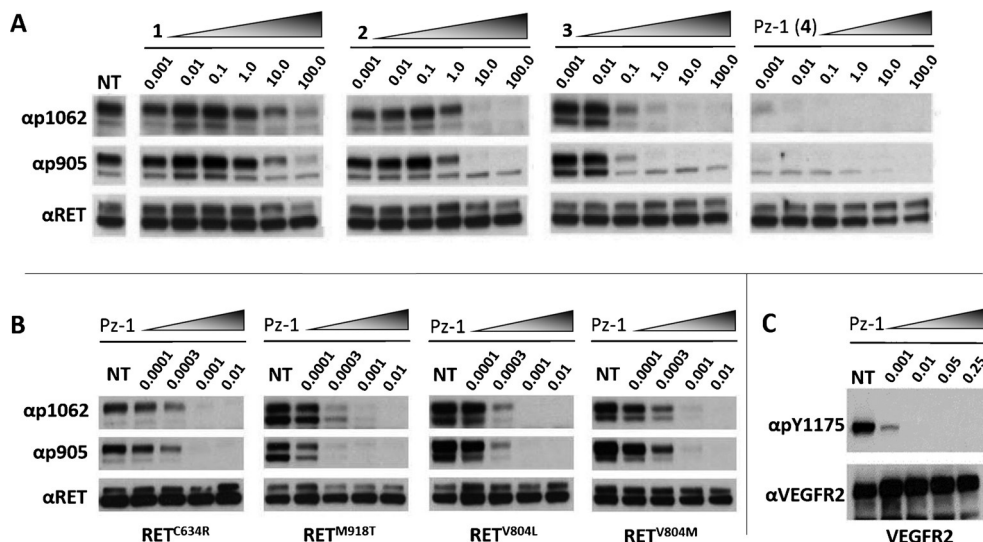

Figure 3. A) SAR evolution from KDF **1** to Pz-1 (**4**). The indicated compounds were tested in cell-based assays (RAT1 fibroblasts transfected with RET^{C634R}); RET phosphorylation (pRET) was measured at two sites (Y1062 and Y905) by immunoblot analysis. Data is reported in micromolar concentrations. B) Pz-1 (**4**) mediated inhibition of pRET in RET-mutant-transfected RAT1 fibroblasts (see A for details). C) Pz-1 mediated inhibition of pVEGFR2 in VEGFR2 transiently transfected HEK293 cells (see A for details). All data is reported in micromolar concentrations. NT = no treatment.

Table S1). Pz-1 preferentially inhibited RET- over Ras-driven tumors (Figure 4). Indeed, whereas this treatment completely prevented the formation of tumors induced by RET^{C634Y}, it reduced, but did not abrogate, the formation of tumors driven by HRas^{G12V} (Figure 4, see also Table S1). Only in RET-driven tumors was Pz-1 able to inhibit MAPK and mTOR mitogenic signaling cascades (Figure S10). Even at a dose of 10.0 mg kg^{-1}, Pz-1 had no effect on MAPK signaling in Ras tumors. However, in both RET- and Ras-driven tumors, Pz-1 (1.0 mg kg^{-1}) inhibited VEGFR2 phosphorylation. The preferential efficacy of Pz-1 for RET-driven tumors may be explained by its dual effect on both the parenchyma (RET) and stroma (VEGFR2) supporting the polypharmacological strategy to target these tumor types. Pz-1 was highly tolerated at daily doses of up to 100.0 mg kg^{-1} for one week in mice (Figure S11). The amount of alanine transaminase (ALT), which can be used as a monitorable toxicity marker, increased in a linear fashion with the Pz-1 dose, but remained
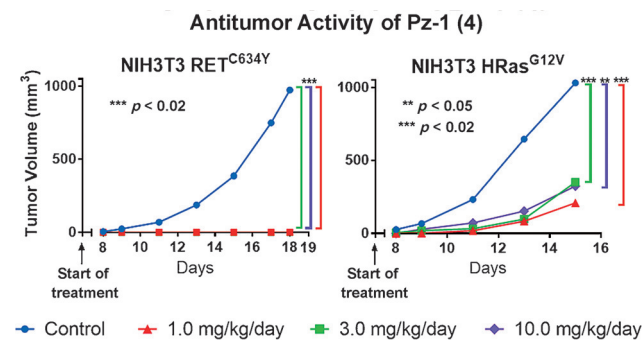
Pz-1 was subjected to kinome screening to determine the global kinase selectivity. At a concentration of 50.0 nM, Pz-1 was screened against a 91 kinase panel representing each kinome cluster (Figure S7). Pz-1 featured good global kinase selectivity with activity on only seven additional kinases (TRKB, TRKC, GKA, FYN, SRC, TAK1, MUSK), which is consistent with the low toxicity that was observed in the cell-based assays (Figure S9).

To address in vivo RET-driven effects, Pz-1 was tested on tumors induced by oncogenic RET that were compared to a constitutively active control Ras oncogene. To this end, NIH3T3 fibroblasts transformed by either RET^{C634Y} or HRas^{G12V} were used. In in vitro cell assays, NIH3T3 RET^{C634Y} cell proliferation was inhibited by Pz-1 with an IC$_{50}$ value of 0.5 nM, a dose significantly lower than that required to inhibit NIH3T3 HRas^{G12V} cell proliferation (IC$_{50}$ = 34.4 nM; Figure S8B). This was paralleled by the efficient inhibition of RET^{C634Y} tyrosine phosphorylation (Figure S8A). At concentrations of up to 100.0 nM, Pz-1 exerted only a minimal growth inhibition on parental NIH3T3 cells (Figure S9).

Immunodeficient (nu/nu) mice were then injected with NIH3T3 RET^{C634Y} or NIH3T3 HRas^{G12V} cells and treated per os with Pz-1 (1.0, 3.0, or 10.0 mg kg^{-1} day^{-1}) before the tumors had appeared, or left untreated (Figure 4; see also

Figure 4. Antitumor activity of Pz-1 (**4**) in nude mice implanted with RET- or Ras-transformed NIH3T3 fibroblasts. NIH3T3 RET^{C634Y} or NIH3T3 HRas^{G12V} cells were inoculated subcutaneously into nu/nu mice. After four days, animals were randomly assigned to receive Pz-1 (1.0, 3.0, or 10 mg kg^{-1} daily) by oral gavage (ca. 7 mice) or left untreated (8 mice). Average tumor volumes are reported. Standard deviations are given in Table S1.

within a normal range (Figure S11). Furthermore, Pz-1 displayed highly favorable pharmacokinetic properties (Table S2).

In summary, we have identified Pz-1 as a dual kinase inhibitor using a KDF library screen in conjunction with

computational modeling. In cell-based assays, 1.0 nM of Pz-1 strongly inhibited tyrosine phosphorylation of VEGFR2 and clinically relevant RET mutants, including those refractory to vandetanib and cabozantinib (RET^{V804M} and RET^{V804L}). Pz-1 completely blocked RET-driven tumor formation at 1.0 mg kg^{-1} with no detectable toxicity at doses of up to 100.0 mg kg^{-1}. The high activity and low toxicity of Pz-1 can be explained by the selective dual inhibition of both RET and VEGFR2. In conclusion, this study validates medicinal chemistry and single-agent polypharmacology methods to guide the development of compounds with well-defined and balanced activities against multiple cancer-relevant targets for synergistic outcomes. The clinical development of Pz-1 may offer a promising therapeutic approach for patients afflicted with RET-driven malignancies and represents a paradigm shift for targeted therapies.

[1] R. Capdeville, E. Buchdunger, J. Zimmermann, A. Matter, *Nat. Rev. Drug Discovery* **2002**, *1*, 493–502.

[2] a) J. Settleman, *Drug Discovery Today Dis. Mech.* **2005**, *2*, 139–144; b) C. C. Smith, Q. Wang, C. S. Chin, S. Salerno, L. E. Damon, M. J. Levis, A. E. Perl, K. J. Travers, S. Wang, J. P. Hunt, P. P. Zarrinkar, E. E. Schadt, A. Kasarskis, J. Kuriyan, N. P. Shah, *Nature* **2012**, *485*, 260–263.

[3] P. Lito, N. Rosen, D. B. Solit, *Nat. Med.* **2013**, *19*, 1401–1409.

[4] a) A. C. Dar, T. K. Das, K. M. Shokat, R. L. Cagan, *Nature* **2012**, *486*, 80–84; b) T. S. Gujral, L. Peshkin, M. W. Kirschner, *Proc. Natl. Acad. Sci. USA* **2014**, *111*, 5048–5053.

[5] a) N. P. Shah, C. Tran, F. Y. Lee, P. Chen, D. Norris, C. L. Sawyers, *Science* **2004**, *305*, 399–401; b) W. Zhou, D. Ercan, L. Chen, C. H. Yun, D. Li, M. Capelletti, A. B. Cortot, L. Chirieac, R. E. Iacob, R. Padera, J. R. Engen, K. K. Wong, M. J. Eck, N. S. Gray, P. A. Jänne, *Nature* **2009**, *462*, 1070–1074; c) M. D. Balbas, M. J. Evans, D. J. Hosfield, J. Wongvipat, V. K. Arora, P. A. Watson, Y. Chen, G. L. Greene, Y. Shen, C. L. Sawyers, *eLife* **2013**, *2*, e00499.

[6] a) L. M. Mulligan, *Nat. Rev. Cancer* **2014**, *14*, 173–186; b) F. Carlomagno, M. Santoro, *Nat. Rev. Endocrinol.* **2011**, *7*, 65–67; c) M. Takahashi, J. Ritz, G. M. Cooper, *Cell* **1985**, *42*, 581–588; d) M. Santoro, F. Carlomagno, A. Romano, D. P. Bottaro, N. A. Dathan, M. Grieco, A. Fusco, G. Vecchio, B. Matoskova, M. H. Kraus, P. P. Di Fiore, *Science* **1995**, *267*, 381–383.

[7] a) W. Pao, K. E. Hutchinson, *Nat. Med.* **2012**, *18*, 349–351; b) P. Ballerini, S. Struski, C. Cresson, N. Prade, S. Toujani, C. Deswarte, S. Dobbelstein, A. Petit, H. Lapillonne, E. F. Gautier, C. Demur, E. Lippert, P. Pages, V. Mansat-De Mas, J. Donadieu, F. Huguet, N. Dastugue, C. Broccardo, C. Perot, E. Delabesse, *Leukemia* **2012**, *26*, 2384–2389; c) T. Wiesner, J. He, R. Yelensky, R. Esteve-Puig, T. Botton, I. Yeh, D. Lipson, G. Otto, K. Brennan, R. Murali, M. Garrido, V. A. Miller, J. S. Ross, M. F. Berger, A. Sparatta, G. Palmedo, L. Cerroni, K. J. Busam, H. Kutzner, M. T. Cronin, P. J. Stephens, B. C. Bastian, *Nat. Commun.* **2014**, *5*, 3116–3122.

[8] a) E. Rizzi, G. Cassinelli, S. Dallavalle, C. Lanzi, R. Cincinelli, R. Nannei, G. Cuccuru, F. Zunino, *Bioorg. Med. Chem. Lett.* **2007**, *17*, 3962–3968; b) R. Graham Robinett, A. J. Freemerman, M. A. Skinner, L. Shewchuk, K. Lackey, *Bioorg. Med. Chem. Lett.* **2007**, *17*, 5886–5893; c) R. Cincinelli, G. Cassinelli, S. Dallavalle, C. Lanzi, L. Merlini, M. Botta, T. Tuccinardi, A. Martinelli, S. Penco, F. Zunino, *J. Med. Chem.* **2008**, *51*, 7777–7787.

[9] a) http://www.fda.gov, Press Announcement No. UCM330143, accessed 26th of January, 2015; b) http://www.fda.gov, Press Announcement No. UCM250168, accessed 26th of January, 2015 (archived); c) S. A. Wells, Jr., B. G. Robinson, R. F. Gagel, H. Dralle, J. A. Fagin, M. Santoro, E. Baudin, R. Elisei, B. Jarzab, J. R. Vasselli, J. Read, P. Langmuir, A. J. Ryan, M. J. Schlumberger, *J. Clin. Oncol.* **2012**, *30*, 134–141; d) F. Carlomagno, D. Vitagliano, T. Guida, F. Ciardiello, G. Tortora, G. Vecchio, A. J. Ryan, G. Fontanini, A. Fusco, M. Santoro, *Cancer Res.* **2002**, *62*, 7284–7290.

[10] a) F. M. Yakes, J. Chen, J. Tan, K. Yamaguchi, Y. Shi, P. Yu, F. Qian, F. Chu, F. Bentzien, B. Cancilla, J. Orf, A. You, A. D. Laird, S. Engst, L. Lee, J. Lesch, Y. C. Chou, A. H. Joly, *Mol. Cancer Ther.* **2011**, *10*, 2298–2308; b) R. Elisei, M. J. Schlumberger, S. P. Müller, P. Schöffski, M. S. Brose, M. H. Shah, L. Licitra, B. Jarzab, V. Medvedev, M. C. Kreissl, B. Niederle, E. E. Cohen, L. J. Wirth, H. Ali, C. Hessel, Y. Yaron, D. Ball, B. Nelkin, S. I. Sherman, *J. Clin. Oncol.* **2013**, *31*, 3639–3646.

[11] a) I. Kufareva, R. Abagyan, *J. Med. Chem.* **2008**, *51*, 7921–7932; b) P. P. Knowles, J. Murray-Rust, S. Kjaer, R. P. Scott, S. Hanrahan, M. Santoro, C. F. Ibanez, N. Q. McDonald, *J. Biol. Chem.* **2006**, *281*, 33577–33587; c) O. Trott, A. J. Olson, *J. Comput. Chem.* **2010**, *31*, 455–461; d) S. Kjaer, S. Hanrahan, N. Totty, N. Q. McDonald, *Nat. Struct. Mol. Biol.* **2010**, *17*, 726–731; e) C. Pargellis, L. Tong, L. Churchill, P. F. Cirillo, T. Gilmore, A. G. Graham, P. M. Grob, E. R. Hickey, N. Moss, S. Pav, J. Regan, *Nat. Struct. Biol.* **2002**, *9*, 268–272.

[12] a) G. E. De Kloe, D. Bailey, R. Leurs, I. J. de Esch, *Drug Discovery Today* **2009**, *14*, 630–646; b) D. Joseph-McCarthy, *J. Comput.-Aided Mol. Des.* **2009**, *23*, 449–451; c) D. C. Rees, M. Congreve, C. W. Murray, R. Carr, *Nat. Rev. Drug Discovery* **2004**, *3*, 660–672; d) P. J. Hajduk, J. Greer, *Nat. Rev. Drug Discovery* **2007**, *6*, 211–219.

[13] a) F. Carlomagno, T. Guida, S. Anaganti, L. Provitera, S. Kjaer, N. Q. McDonald, A. J. Ryan, M. Santoro, *Endocr.-Relat. Cancer* **2009**, *16*, 233–241; b) F. Carlomagno, T. Guida, S. Anaganti, G. Vecchio, A. Fusco, A. J. Ryan, M. Billaud, M. Santoro, *Oncogene* **2004**, *23*, 6056–6063; c) L. Mologni, S. Redaelli, A. Morandi, I. Plaza-Menacho, C. Gambacorti-Passerini, *Mol. Cell. Endocrinol.* **2013**, *377*, 1–6.